ELSEVIER

Journal of Power Sources 102 (2001) 46–54

JOURNAL OF POWER SOURCES

www.elsevier.com/locate/jpowsour

Solid-state rechargeable magnesium cell with poly(vinylidenefluoride)–magnesium triflate gel polymer electrolyte

G. Girish Kumar, N. Munichandraiah*

Department of Inorganic and Physical Chemistry, Indian Institute of Science, Bangalore 560012, India

Received 22 January 2001; received in revised form 19 March 2001; accepted 21 March 2001

Abstract

A gel polymer electrolyte (GPE) film of poly(vinylidenefluoride) and magnesium triflate is prepared and studied for application in a solid-state rechargeable magnesium battery. The composition of GPE is optimized in view of minimum liquid components and maximum specific conductivity (σ). The σ of GPE of optimum composition is 2.67×10^{-3} S cm^{-1} at 20°C, and it follows a Vogel, Tamman and Fulcher equation with an activation energy of about 0.4 kJ mol^{-1}. The effect of aging on the Mg/GPE interface is studied. The formation of a passivating film on the Mg surface, which increases in thickness on aging in GPE, is established. Several Mg/GPE/MnO_2 cells are assembled and studied for discharge capacity and cyclic-life data. The results reveal that Mg/GPE/MnO_2 cells at *C*/8, *C*/6 and *C*/4 discharge rates yield, respectively, capacities of 160, 80 and 50 mAh g^{-1} of MnO_2. These values are nearly constant for about 30 cycles. Further cycling of the cells leads to a decrease in capacity, which is attributed to passivation of the magnesium electrode and poor efficiency of the Mg^{2+} ion insertion into the MnO_2 positive electrode.

Keywords: Solid-state Mg/MnO_2 cell; Gel polymer electrolyte; VTF equation; Alternating current impedance spectroscopy; Cyclic voltammetry; Cycle-life

1. Introduction

The need for high performance and environmental-friendly batteries has been a major interest for the development of novel electrochemical systems. At present, research efforts are directed towards several aspects of Li-ion batteries, namely, enhancing performance and scaling-up to large-size units [1]. Magnesium is an attractive electrode material with a potential of −2.3 V versus SHE. The metal is positioned next to lithium in the EMF series and its electrochemical equivalence (2.2 Ah g^{-1}) is also high. It has been studied as a negative electrode in primary and reserve batteries, which are based on aqueous electrolytes [2]. Studies related to the development of secondary magnesium batteries are limited. Investigations on rechargeable magnesium batteries are interesting on many accounts in comparison with Li batteries, namely: (i) the ionic radii of Li^+ and Mg^{2+} are 68 and 65 pm, respectively, which are comparable in magnitude [3], hence, easy replacement of Li^+ ions by Mg^{2+} ions in insertion compounds is possible; (ii) Mg metal is more stable than Li, i.e. can be handled safely in oxygen and humid atmospheres unlike Li, which requires an argon or helium atmosphere of high purity, consequently, safety problems arising from a rechargeable Mg battery are minimal; (iii) global raw material resources are plentiful, and, hence, Mg is much cheaper than Li, the resources of which are limited and localized. Owing to these merits, investigations on the electrochemistry of Mg-based rechargeable battery systems assume significant importance. Thus, a solid-state battery employing Mg as the anode attracts considerable interest. In 1990, Gregory et al. [4] reported an attempt to construct a rechargeable Mg battery based on a Mg_xCoO_y intercalation cathode. Recently, Aurbach et al. [5] have developed a prototype rechargeable magnesium battery. Nevertheless, investigations on solid-state rechargeable magnesium batteries are scarce in the literature [6]. We have reported studies on a solid-state Mg/MnO_2 cell which employed a gel polymer electrolyte (GPE) of polyacrylonitrile [7]. In the present study, we investigate a GPE of poly(vinylidineflouride) and the results of characterization as well as assembly and evaluation of a solid-state Mg/GPE/MnO_2 cell are reported.

2. Experimental

Propylene carbonate (PC), ethylene carbonate (EC) and magnesium trifluoromethanesulfonate (magnesium triflate,

* Corresponding author. Tel.: +91-80-309-2828; fax: +91-80-3600683.
E-mail address: muni@ipc.iisc.ernet.in (N. Munichandraiah).

0378-7753/01/$ – see front matter
PII: S0378-7753(01)00772-8

MgTr) were purchased from Aldrich. Poly(vinylidenefluoride) (PVDF) was purchased from Fluka. The solvents PC and EC were vacuum distilled at 110°C, and MgTr was vacuum dried at 100°C before use. A suspension which contained the required quantities of PVDF, PC, EC and MgTr in a glass petri-dish was heated at about 100°C for about 2 min. On cooling, a GPE film formed. Equal quantities by weight of PC and EC were used in all experiments. For the purpose of arriving at an appropriate composition, several GPE films were prepared by varying the quantities of (PC + EC) and MgTr in a constant quantity of PVDF. Circular specimens (area = 0.8 cm^2) of magnesium were sectioned out of a sheet of Mg AZ21 alloy (DOW Chemical Company). These specimens were polished with successive grades of emery paper to a smooth finish, washed thoroughly in water, rinsed in acetone and dried at ambient conditions.

Symmetrical cells, SS/GPE/SS and (SS)Mg/GPE/Mg(SS), where SS is stainless steel, were assembled in Teflon holders and contained in air-tight glass containers, which were provided with electrical leads. The manganese dioxide electrodes were prepared using battery grade γ-MnO_2 (electrolytic manganese dioxide, EMD). A mixture of EMD (80 wt.%), graphite powder (10 wt.%) and PVDF (10 wt.%) of the GPE composition as the binder was thoroughly ground in a mortar and applied to a nickel grid (10 mm × 10 mm). The nickel grid was subjected to prior degreasing in alkali and etching in dilute HCl. The grid, together with the electrode material, was heated at 70°C for about 3 min and then compacted at a pressure of 10 tonnes cm^{-2}. A Mg/GPE/MnO_2/GPE/Mg cell (for brevity, hereafter referred to as a Mg/GPE/MnO_2 cell) was assembled by sandwiching the respective electrodes and the GPE film in a sealed container. Several cells were constructed for the purpose of different experiments and to ensure reproducibility. The ambient temperature of the cells was maintained at 20 ± 1°C in an air-conditioned room.

Temperature-dependent experiments were conducted in the temperature range between −6 and 20°C using a Julabo programmable refrigerator (model HP4). For the purpose of experiments at temperatures greater than 20°C, the cells were heated by means of an electrical heating tape (which surrounded the glass container), a thermocouple and a temperature controller. The temperature inside the glass container was measured to an accuracy of ±1°C. The symmetrical cells were subjected to ac impedance measurements using an electrochemical impedance analyzer (EG&G PARC model 6310) in the frequency range 100 kHz to 5 mHz with an excitation signal of 5 mV. The impedance data were analyzed by using an equivalent circuit and a non-linear least squares (NLLS) fitting program [8], as in an earlier study [9]. Cyclic voltammograms were recorded at a sweep rate of 5 mV s^{-1} using a potentiostat/galvanostat (EG&G PARC model Versastat). Charge/discharge cycling of the Mg/GPE/MnO_2 cells was carried out using a galvanostat/potentiostat (Autolab model 30) or a galvanostatic circuit, which consisted of a regulated dc power source, a high resistance and an ammeter in series. The cell voltage was measured using a Philips multimeter model PP9007.

3. Results and discussion

3.1. Alternating current impedance of SS/GPE/SS cell

The ac impedance spectrum of a SS/GPE/SS symmetrical cell with a GPE of arbitrary composition is shown in both Nyquist and Bode forms in Fig. 1. The response of the cell can be understood on the basis of the equivalent circuit shown in Fig. 2(a). The impedance (Z) of the cell is given by

$$Z = \left(R_b - \frac{j}{2\pi f C_g}\right) + \left(R_i - \frac{j}{2\pi f C_i}\right) \quad (1)$$

where R_i and R_b are the resistance of the SS/GPE inter-phase and the resistance of the GPE, respectively, and C_i and C_g the capacitance of the SS/GPE inter-phase and the geometric

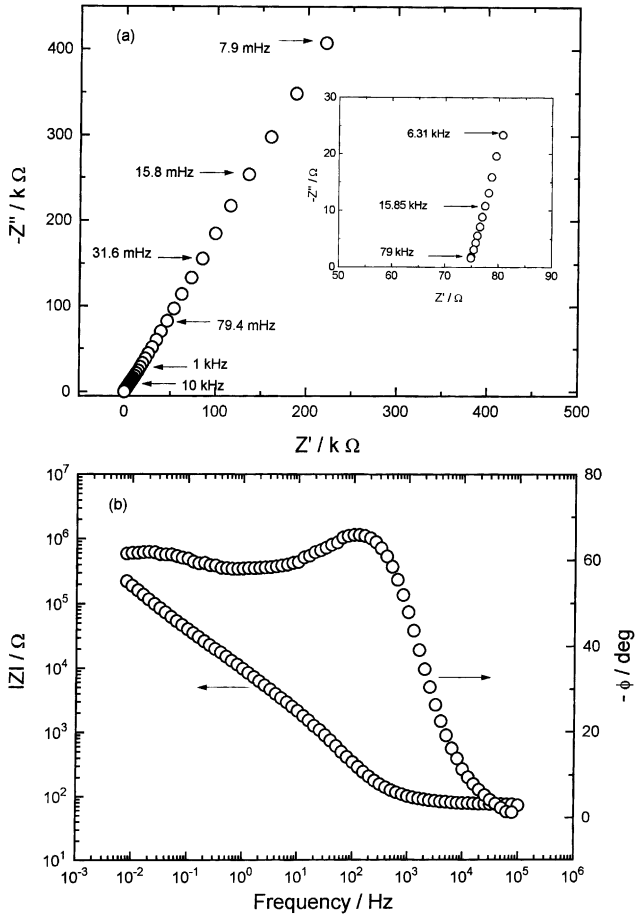

Fig. 1. Alternating current impedance spectrum in (a) Nyquist, and (b) Bode forms of SS/GPE/SS cell at 20°C. Symbols: Z', Z'', |Z|, and ϕ refer to real component, imaginary component, modulus, and phase angle, respectively. High-frequency data of the Nyquist spectrum is expanded and shown in inset. Frequency values for some data points are given. Thickness of GPE = 0.85 mm and area of SS electrode = 0.56 cm^2.

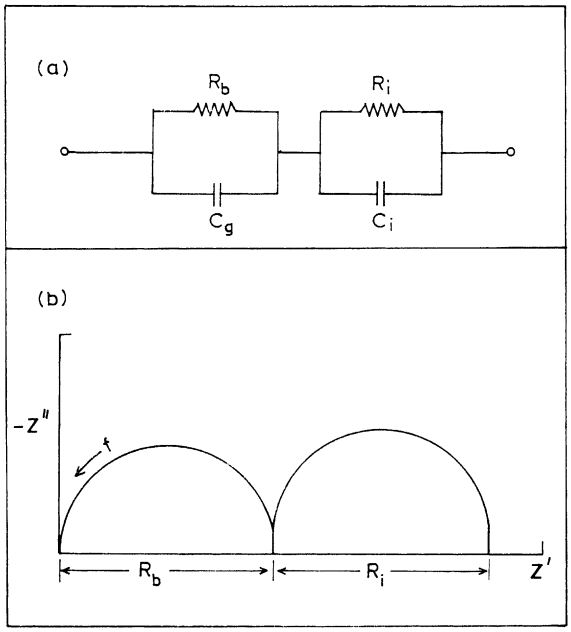

Fig. 2. (a) Electrical equivalent circuit of SS/GPE/SS cell, and (b) corresponding Nyquist impedance spectrum. Symbols R_b and R_i refer to resistance of GPE and resistance of SS/GPE inter-phase; C_g and C_i refer to capacitance of GPE and capacitance of SS/GPE inter-phase, respectively.

capacitance of the GPE, respectively; f the ac frequency. On the right-hand side of Eq. (1), the impedance of the GPE is given in the first parenthesis and the impedance of the inter-phase is given in the second parenthesis. A schematic impedance spectrum, which is expected theoretically from Eq. (1) is shown in Fig. 2(b) with two semicircles. The frequency range of each semicircle depends on the RC time-constant of the resistance and the capacitance pair. From published information on lithium-based solid polymer electrolytes, the high-frequency semicircle is attributed to the polymer electrolyte and the low-frequency semicircle to the inter-phase.

The experimental spectrum in Fig. 1(a) shows that the high-frequency semicircle corresponding to the GPE is absent and the data corresponding to the SS/GPE inter-phase has not taken the shape of a semicircle. The fact that the high-frequency intercept of the data on the real axis is at about 75 Ω instead of the origin of the plot suggests that the GPE semicircle may appear in a frequency range higher than 100 kHz. Since the equipment employed for the present experiments has a frequency limitation of 100 kHz, experiments could not be conducted at a higher frequency range. Therefore, the impedance data encompass only the SS/GPE inter-phase and the linearity of the data indicates a high value for R_i. This is due to the fact that the SS behaves as a blocking electrode and, therefore, offers a high resistance for electron-transfer across the SS/GPE interface. The resistance (R_b) of the GPE is obtained from the intercept of the high-frequency data on the real axis. For the purpose of evaluating R_i, the Bode representation of the impedance (Fig. 1(b)) is useful. The total cell resistance (R_t) can be obtained from the low-frequency intercept of the impedance modulus (|Z|) (Fig. 1(b)). R_i can be obtained from

$$R_i = R_t - R_b \quad (2)$$

The capacitive behavior of the SS/GPE/SS is evident from the magnitude of the phase angle, which is between −65 and −70° over the frequency range 100–0.005 Hz (Fig. 1(b)).

3.2. Conductivity and composition of GPE

The specific conductance (σ) of the GPE is calculated as follows:

$$\sigma = \frac{l}{AR_b} \quad (3)$$

where l is thickness of the GPE, A the area of the SS electrode. A σ value of 2.02×10^{-3} S cm^{-1} at 20°C is obtained from the data in Fig. 1.

The value of σ for a PEO-based, solvent-free, SPE film is about 1×10^{-8} S cm^{-1} at ambient temperature, which is very low for any battery application. On the other hand, the GPE of PVDF exhibits higher ionic conductivity due to the presence of a solution of MgTr dissolved in PC and EC as solvents. The mechanical strength of the GPE film, however, is rather poor due to the presence of the solvent, unlike the solvent-free SPE, which possesses good mechanical strength. To prepare a GPE film with good mechanical strength, it is considered that the liquid components (viz. PC and EC) should be at a minimum level. Thus, a series of GPE films were prepared by varying the quantity of PC and EC with a fixed mass ratio of PVDF to MgTr, and σ values were measured (Table 1).

For a convenient formation of the gel, the mass ratio of (PC + EC) to PVDF is found to be 4:1. With this ratio of (PC + EC) to MgTr, several GPE films were prepared by varying the concentration of MgTr. The variation in σ with MgTr concentration at 20°C is shown in Fig. 3. At low concentrations of MgTr, σ is about 1.44×10^{-3} S cm^{-1} and increases with concentration to reach a maximum value of about 2.67×10^{-3} S cm^{-1}. This is due to the increase in Mg^{2+} ion concentration. Further increase in the concentration of MgTr results in a decrease in σ, probably due to ion-pair formation. Thus, the maximum value of σ obtained is 2.67×10^{-3} S cm^{-1} at 20°C for a PVDF:PC:EC:MgTr mass ratio of 1:2:2:0.8. The GPE films studied for the

Table 1
Specific conductivity (σ) of gel polymer electrolytes containing PVDF (0.5 g), MgTr (0.2 g) and different masses of (PC + EC) at 20°C

Mass of (PC + EC) (g)	σ (S cm^{-1})
1.0	8.894×10^{-4}
1.5	1.411×10^{-3}
2.0	1.889×10^{-3}
2.5	2.301×10^{-3}

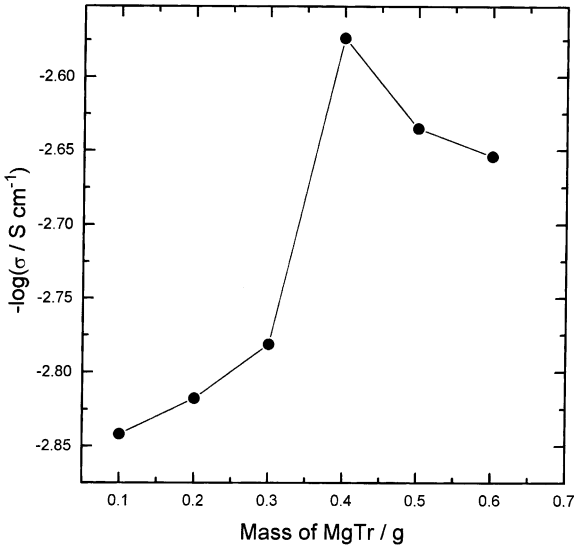

Fig. 3. Specific conductivity (σ) of GPE as function of mass of MgTr in PVDF (0.5 g), PC (1.0 g) and EC (1.0 g) at 20°C.

purpose of composition optimization are shown in Fig. 4, which includes the variation of mass fraction of PVDF, PC + EC and MgTr. The GPE film of optimum composition is indicated by a closed circle.

For the purpose of temperature dependence studies of σ, SS/GPE/SS cells with different concentrations of MgTr in GPE were subjected to ac impedance measurements at several temperatures between −6 and 50°C and σ values were calculated. Examination of the literature on SPEs of several salts suggests that Arrhenius as well as non-Arrhenius types of ionic conduction are observed in different cases. This depends on the type of salt and the temperature range [10]. The variation of the σ of GPE with inverse of temperature is shown in Fig. 5. The value of the σ is 8.34×10^{-4} S cm^{-1} at −6°C; it increases non-linearly and reached a value of 3.43×10^{-3} S cm^{-1} at 50°C. The non-Arrhenius conduction behavior of a GPE is generally

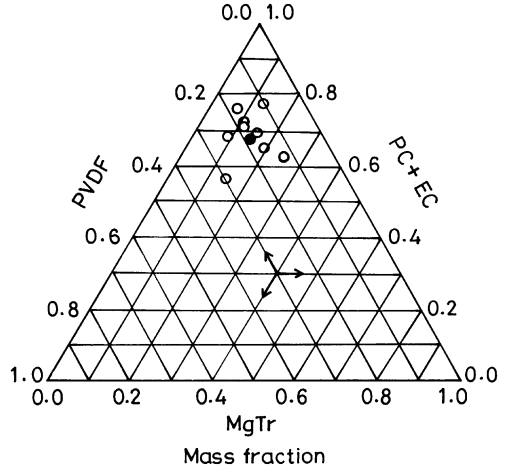

Fig. 4. Composition diagram of GPE films studied for optimization purposes. Solid circle indicates optimum composition.

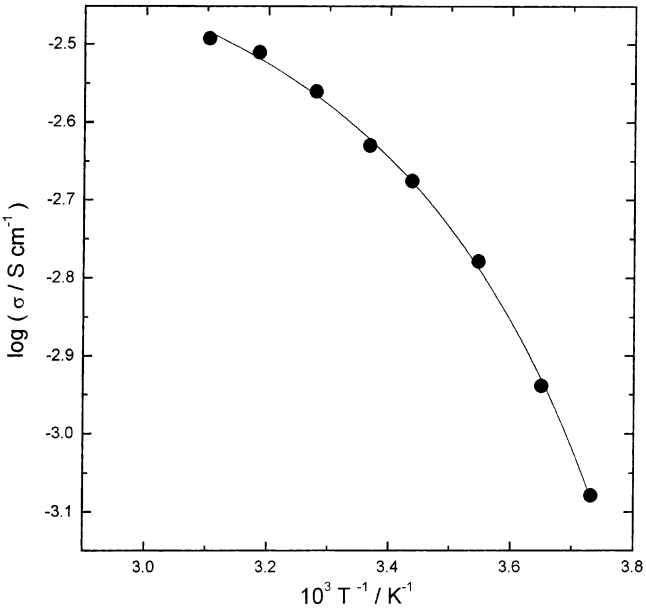

Fig. 5. Temperature-dependence (Arrhenius diagram) of specific conductivity (σ) of GPE film of optimum composition.

explained on the basis of VTF theory. Accordingly, the relationship between σ and T is given by

$$\sigma = A_0 T^{-1/2} \exp\left(\frac{-E_a}{(T - T_0)}\right) \quad (4)$$

where the constant A_0 is assumed to be independent of temperature, and T_0 the equilibrium glass-transition temperature, which is close to the glass-transition temperature (T_g) of the GPE. The conductivity data were analyzed to evaluate A_0, T_0 and E_a by means of NLLS fitting procedures. The theoretical curves generated from the fit results are shown as a solid curve in Fig. 5. The value of E_a obtained for the GPE of optimum composition is 0.4 kJ mol^{-1}.

3.3. Cyclic voltammetry

The SS/GPE/SS and Mg/GPE/Mg symmetrical cells were subjected to cyclic voltammetry, the voltammograms are shown in Fig. 7. The magnitude of current through the SS/GPE/SS cells is very low and there are no current peaks in the voltammograms. On the other hand, well-defined cathodic and anodic peaks are present in the voltammograms for the Mg/GPE/Mg cells. These results indicate that the cathodic deposition of Mg is not favored on SS, whereas the reaction

$$Mg^{2+} + 2e^- \rightleftharpoons Mg \quad (5)$$

is facile at the interface between Mg and GPE. The potentials of the cathodic and anodic peaks are separated by more than 30 mV, which is to be expected for a two electron-transfer reaction. This is due to the fact that there is no reference electrode present in the cell; difficulties involved

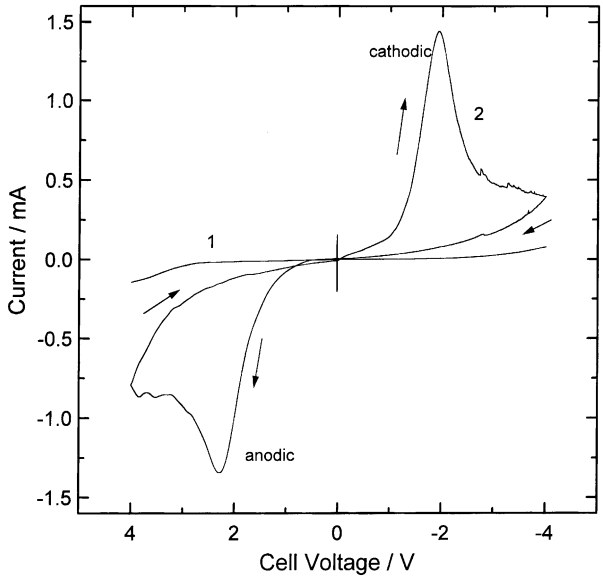

Fig. 6. Cyclic voltammogram of: (i) SS/GPE/SS cell; (2) a Mg/GPE/Mg cell. In both cases, scan rate = 5 mV s^{-1}, temperature = 20°C, and thickness of GPE = 0.35 mm. Area of SS electrode = 0.5 cm^2; area of the Mg electrode = 1.0 cm^2.

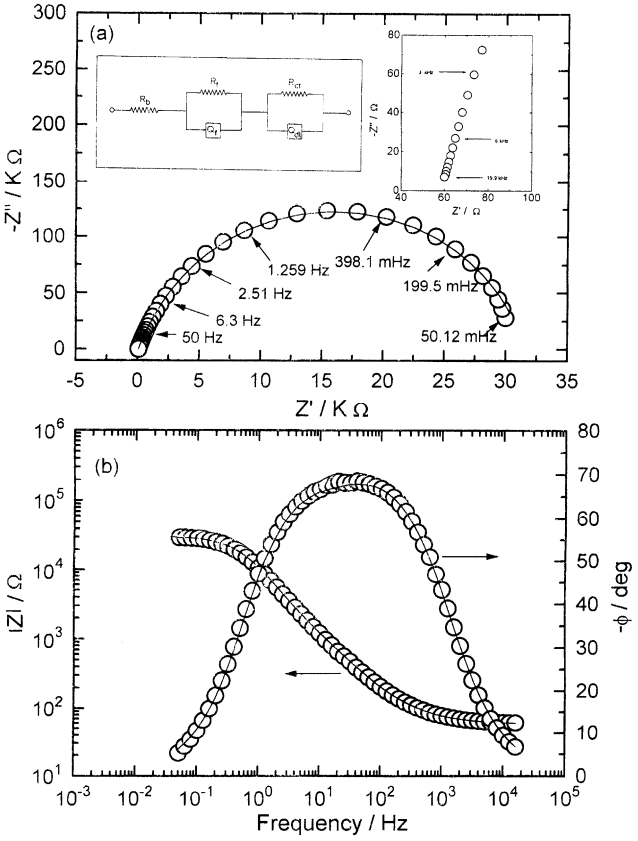

Fig. 7. Alternating current impedance data as (a) Nyquist plot and (b) Bode plot of a Mg/GPE/Mg symmetrical cell at 20°C. High-frequency region expanded and shown separately as an inset. Resistance of GPE film (R_Ω = 58 Ω), resistance of surface film on Mg (R_f = 240 Ω) and charge-transfer resistance of $Mg = Mg^{2+} + 2e^-$ reaction (R_{ct} = 32.46 kΩ) are obtained by fitting experimental data to equivalent circuit shown in inset. Q_f and Q_{dl} refer to constant phase elements corresponding to surface film capacitance (C_f) and double-layer capacitance (C_{dl}), respectively. Area of Mg electrode = 1.0 cm^2; thickness of GPE = 1.5 mm. Experimental data are shown as open circles and theoretical data as solid curves.

in introducing a reference electrode into a thin-film of polymer electrolyte have been discussed earlier [11]. Since the reference electrode terminal and counter electrode terminal of the potentiostat were shorted, both the electrodes of the symmetrical cell were polarized, which resulted in a large difference between the peak potentials (ΔE_p). The ohmic drop arising from the resistance of the gel polymer electrolyte is also included in the magnitude of ΔE_p [11]. The ratio of the cathodic charge to the anodic charge is about 0.84. The Mg electrode reaction, Eq. (5), is thus, quasi-irreversible, which perhaps can be attributed to the presence of surface film on the Mg metal.

3.4. Mg/GPE impedance

The impedance spectrum of a Mg/GPE/Mg symmetrical cell with an optimized composition of the GPE is shown in Fig. 7. The Nyquist plot (Fig. 7(a)) takes the shape of a semicircle, unlike the linear data of the SS/GPE/SS cell given in Fig. 1. The high-frequency intercept on the real axis, which is shown as an inset (Fig. 7(a)), provides the value of R_b of the GPE. The σ values obtained from the impedance data of SS/GPE/SS Mg/GPE/Mg cells are nearly the same in magnitude. The semicircle of Fig. 7(a), however, is depressed and elongated which suggests the presence of a pair of overlapping semicircles. The interfacial resistance (R_i) at the Mg/GPE interface, as obtained from the low-frequency intercept of Fig. 7(a), is significantly lower than that of the SS/GPE interface. Furthermore, the interfacial phenomena are composed of two processes as reflected by the overlapping semicircles. It is recognized that alkali and alkaline earth metals are covered with surface films, which impart kinetic stability to the underlying metals. When such a metal is in contact with an electrolyte (either liquid or solid), the surface film, called the solid electrolyte inter-phase (SEI), acts as an interface between the metal and the electrolyte [12]. Thus, the Mg/GPE inter-phase is characterized by the surface film resistance (R_f) and its capacitance (C_f), as well by the charge-transfer resistance (R_{ct}) of reaction (5) and the double-layer capacitance (C_{dl}). The impedance data of Mg/GPE/Mg cells were analyzed for the values of R_b, R_f, C_f, R_{ct} and C_{dl} by a non-linear least squares fitting program which employed the equivalent circuit shown in the inset of Fig. 7(a). Since the semicircles were not perfect, the capacitances were substituted by constant phase elements (CPE) Q_f and Q_{dl}. A CPE is defined in the admittance by

$$Y^* = Y_0(j\omega)^n \quad (6)$$

For $n = 0$, the CPE represents a resistance with $R = Y_0^{-1}$; for $n = 1$, a capacitance with $C = Y_0$; for $n = 0.5$, a Warburg for

$n = -1$, an inductance with $L = Y_0^{-1}$ [8]. The values of the parameters are given in the caption and the theoretical curves are shown as solid lines in Fig. 7. It is seen that the experimental data and the theoretical curves agree well in the both Nyquist (Fig. 7(a)) and Bode (Fig. 7(b)) plots.

The Butler-Volmer relationship between current density (i) and overpotential (η) is generally considered to be valid for an electrochemical reaction also in a SPE medium [11], i.e.

$$i = i_0(e^{-2\alpha F\eta/RT} - e^{2(1-\alpha)F\eta/RT}) \quad (7)$$

Eq. (7) is written for reaction (5). The symbols have their usual meanings. Since the ac excitation signal used for measuring the impedance data was only 5 mV, Eq. (7) can be approximated to

$$i_0 = \frac{-RT}{2FR_{ct}} \quad (8)$$

where $R_{ct} = (-d\eta/di)$ is the charge-transfer resistance. From the value of 64.92 kΩ cm^2 of R_{ct} from Fig. 7, the exchange current density of reaction (2) obtained is 0.2 μA cm^{-2}.

3.5. Aging of Mg/GPE/Mg cells

A symmetrical Mg/GPE/Mg cell was assembled and its ac impedance spectra were recorded at several intervals of aging, as shown in Fig. 8. The size of the semicircle increases with aging as observed in earlier work [13]. The variation of impedance parameters with aging time are shown in Fig. 9. Initially, the resistance R_b of the GPE film is nearly constant with minor fluctuations, as shown in Fig. 9(a). After 200 h, the value of R_b increases slightly and, accordingly, σ decreases (Fig. 9(d)). This can be attributed to loss of solvent (EC + PC) from the gel on aging. An increasing trend for R_f and R_{ct} is seen in Fig. 9(b) and (c), respectively, which is an indication of the growth of the surface film on aging.

3.6. Mg/GPE/MnO_2 cell

Since the GPE of PVDF–MgTr possesses good specific conductivity (2.67×10^{-3} S cm^{-1}) at ambient temperature, and the Mg electrode shows reversibility, as demonstrated by cyclic voltammetry (Fig. 6), cells were assembled with Mg as the negative electrode and MnO_2 as the positive electrode, and with GPE as the electrolyte.

The cyclic voltammogram for the MnO_2 electrode is shown in Fig. 10. A reduction peak appears at a cell voltage of about 1.1 V in the forward scan and an oxidation peak at 2.7 V in the reverse scan. The charge associated with the latter peak is only 50% of that for the former peak. This indicates poor reversibility of the MnO_2 electrode.

The open-circuit voltage of the Mg/GPE/MnO_2 cell was about 2.0 V. After assembly, the cell was allowed to equilibrate under open-circuit conditions for about 4 h before it

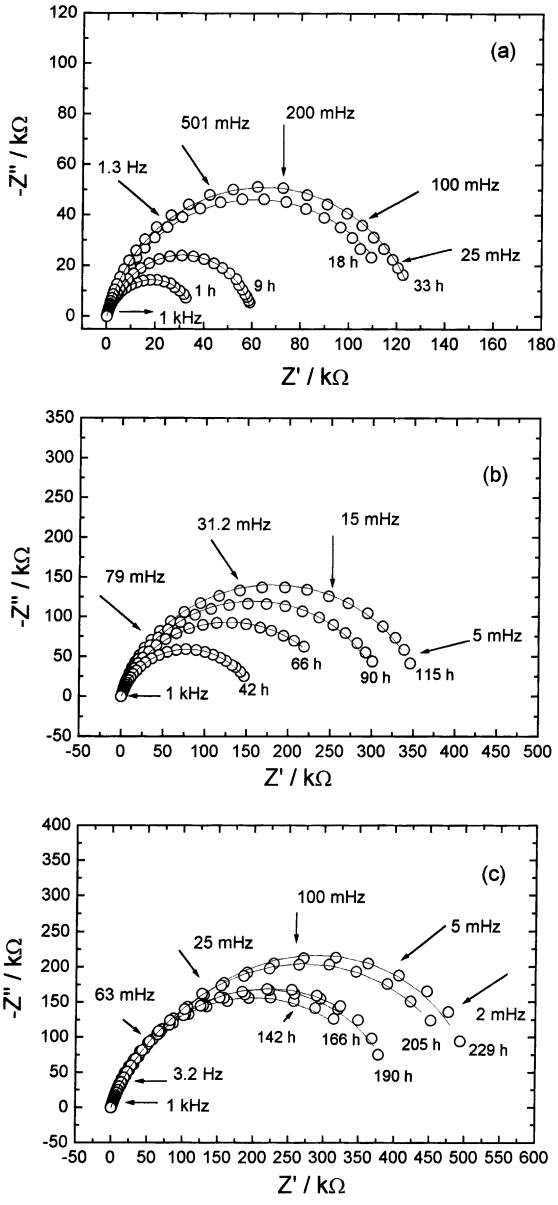

Fig. 8. Nyquist plots of Mg/GPE/Mg cell at different intervals of aging at 20°C. Experimental data shown as open circles and theoretical data from NLLS fit results shown as solid curves. Thickness of GPE film = 0.4 mm; area of Mg electrode = 1.0 cm^2.

was subjected to experimentation. During this period, the cell voltage remained virtually constant. In our earlier studies on GPE made of polyacrylonitrile [7], it was found that the cell exhibits two voltage plateaux during discharge [7]. The first voltage plateau appears above 1.0 V and the second one below 1.0 V. Akin to the reactions involved in a Li–MnO_2 cell with a non-aqueous liquid electrolyte [14], the following reactions are considered to correspond to the voltage plateaux of the Mg/GPE/MnO_2 cell discharge:

$$2MnO_2 + Mg^{2+} + 2e^- \rightarrow [2MnO_2{}^-Mg^{2+}] \quad (9)$$

$$[2MnO_2{}^-Mg^{2+}] + Mg^{2+} + 2e^- \rightarrow 2[MnO_2{}^{2-}Mg^{2+}] \quad (10)$$

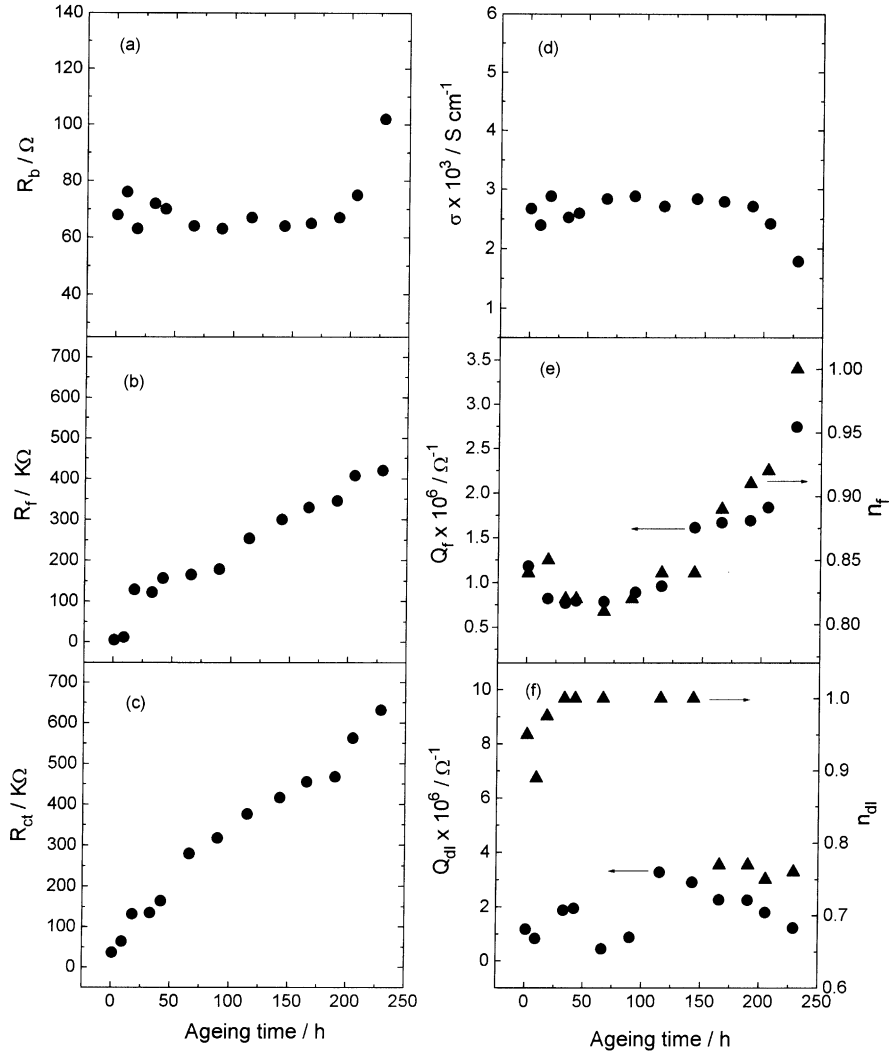

Fig. 9. Variation of impedance parameters of Mg/GPE/Mg cell with aging time. Thickness of GPE film = 0.4 mm; area of Mg electrode = 1.0 cm^2.

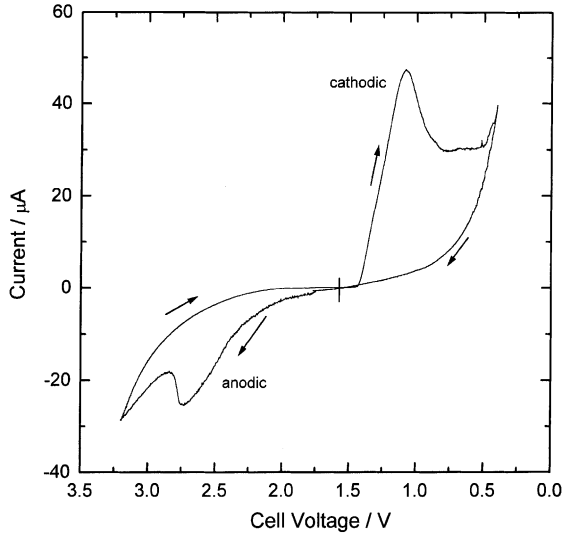

Fig. 10. Cyclic voltammogram at 0.1 mV s^{-1} scan rate of MnO_2 electrode in Mg/GPE/MnO_2 cell at 20°C. Thickness of GPE film = 0.3 mm; electrode area = 1.0 cm^2; mass of MnO_2 = 3 mg.

Reaction (9), which corresponds to the first discharge plateau, is the reduction of MnO_2 from Mn^{4+} to Mn^{3+}. This is accompanied by insertion of Mg^{2+} ions from the GPE into the MnO_2 lattice, which results in the formation of ($2MnO_2^-$ Mg^{2+}). This product undergoes further reduction from Mn^{3+} to Mn^{2+} in reaction (10), which corresponds to the second voltage plateau. Since the cell could not be recharged after discharge to below 1.0 V, a discharge cut-off voltage of 1.1 V was employed.

A typical charge–discharge curve for the Mg/GPE/MnO_2 cell at the *C*/8 rate is shown in the Fig. 11. As the cell was assembled in a charged state, it was discharged first and then charged. The discharge capacity obtained from Fig. 12 is 160 mAh g^{-1} of MnO_2. During charge–discharge cycling, the cell was charged at *C*/8 rate with the same amount of charge that was withdrawn during the previous discharge. In the initial cycles, the charging cut-off voltage was about 3.2 V. This voltage gradually increased, however, with an increase in number of cycles. This is attributed to the growth of a passive film on Mg. Furthermore, it was found that the

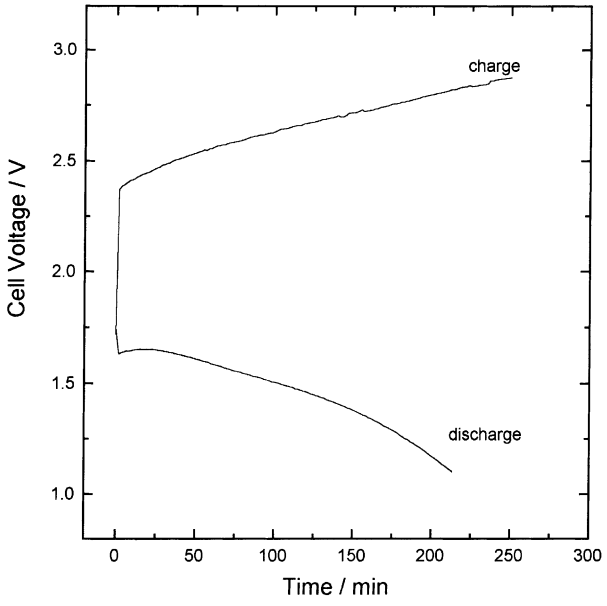

Fig. 11. Variation of voltage of Mg/GPE/MnO_2 cell during charging and discharging with current of 50 μA (approximately *C*/4 rate). Thickness of GPE film = 0.12 mm; electrode area = 1.0 cm^2; mass of MnO_2 = 3 mg.

cell exhibits delay-time behavior akin to that of aqueous batteries of Mg [15]. Cycling of the cells was terminated upon reaching a charging voltage of 4.5 V. Several Mg/GPE/MnO_2 cells were assembled and subjected to charge–discharging cycling at different rates.

The cycle-life data of Mg/GPE/MnO_2 cells at various discharge rates are shown in Fig. 12. A constant capacity of about 160 mAh g^{-1} of MnO_2 is obtained for about 30 cycles at the *C*/8 rate, whereas values of 80 and 50 mAh g^{-1} are

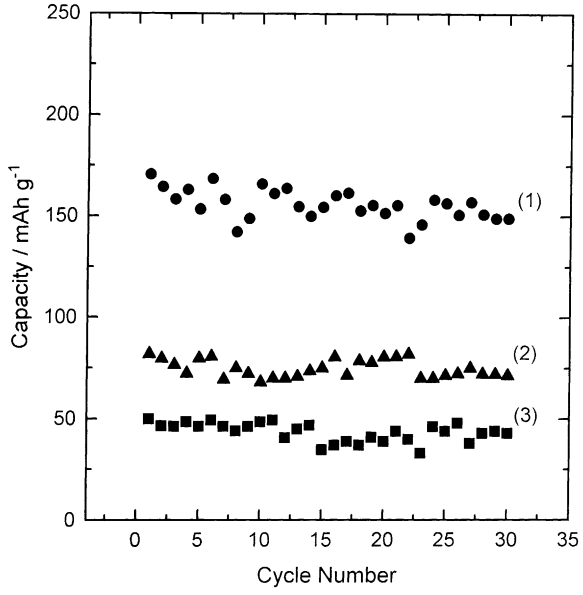

Fig. 12. Cycle-life data of Mg/GPE/MnO_2 cells at (1) *C*/8, (2) *C*/6, (3) *C*/4 rate.

obtained at a *C*/6 and a *C*/4 discharge rate, respectively. The decrease in capacity at higher currents may be attributed to less efficient intercalation of Mg^{2+} ions into the MnO_2. After about 30 cycles, the capacity started to decrease slowly. Two main problems prevented further cycling of the cell, namely: (i) the voltage exceeded 4.5 V, which falls outside the voltage stability window of GPE; (ii) the cell delay-time increased, which was due to increased passivation of the Mg electrode.

4. Conclusions

As PVDF-based gel polymer electrolytes are presently used in the majority of lithium-polymer battery technologies, a gel polymer electrolyte film of PVDF and magnesium triflate is prepared and characterized for application in solid-state rechargeable magnesium batteries. The composition of the GPE is optimized with respect to the minimum amount of liquid components (propylene carbonate and ethylene carbonate) required for gel formation and maximum conductivity. The specific conductivity of the GPE of optimum composition is 2.67 mS cm^{-1} compared with a value of 1.9 mS cm^{-1} obtained for GPE based on polyacrylonitrile [7]. The conduction mechanism of the latter gel was found to follow the Arrhenius relationship. This is not the case, however, for PVDF gel polymer electrolytes. The conductivity data of the PVDF gel polymer electrolytes are found to fit the VTF relationship and, accordingly, the activation energy of conduction is evaluated. Similar VTF behavior, which is uncommon for gel polymer electrolytes, has been reported recently for a PVDF–lithium salt system [16]. Several solid-state Mg/GPE/MnO_2 cells have been assembled and evaluated for discharge capacity and cyclic-life data. Discharge capacity values as high as 150 mAh g^{-1} of MnO_2 are obtained against a value of about 20 mAh g^{-1} reported [7]. The discharge capacity is nearly constant for about 30 cycles. Further cycling of the cells leads to a decrease in capacity, which is attributed to the passivation of the magnesium electrode and poor efficiency of the Mg^{2+} ion insertion into the MnO_2 positive electrode.

Acknowledgements

Financial support from the Council of Scientific and Industrial Research, Government of India, Project no. 01 (1505)/98/EMR-II, is gratefully acknowledged.

References

[1] P. Novak, M. Winter, Adv. Mater. 10 (1998) 725.
[2] J.L. Robinson, in: N.C. Cahoon, G.W. Heise (Eds.), The Primary Battery, Vol. II, Wiley, New York, 1976, p. 149.
[3] A. Patrick, M. Glasse, R. Lathem, R. Linford, Solid State Ionics 18 & 19 (1986) 1063.

[4] T.D. Gregory, R.J. Hoffman, R.C. Winterton, J. Electrochem. Soc. 137 (1990) 775.
[5] D. Aurbach, Z. Lu, A. Schechter, Y. Gofer, H. Gizbar, R. Turgeman, Y. Cohen, M. Moshkovich, E. Levi, Nature 274 (2000) 724.
[6] P. Novak, R. Imhof, O. Haas, Electrochim. Acta 45 (1999) 351.
[7] G. Girish Kumar, N. Munichandraiah, J. Power Sources 91 (2000) 157.
[8] B.A. Boukamp, Equivalent Circuit Manual, University of Twente, AE Enechede, 1989, p. 1.
[9] N. Munichandraiah, L.G. Scanlon, R.A. Marsh, J. Power Sources 72 (1998) 203.
[10] M.B. Armand, in: J.R. MacCallum, C.A. Vincent (Eds.), Polymer Electrolyte Reviews, Vol. 1, Elsevier, London, 1987, p. 1.
[11] N. Munichandraiah, L.G. Scanlon, R.A. Marsh, B. Kumar, A.K. Sircar, J. Electroanal. Chem. 379 (1994) 495.
[12] E. Peled, in: J.P. Gabano (Ed.), Lithium Batteries, Academic Press, London, 1983, p. 43.
[13] G. Girish Kumar, N. Munichandraiah, Solid State Ionics 128 (2000) 203.
[14] H. Ikeda, in: J.P. Gabano (Eds.), Lithium Batteries, Academic Press, London, 1983, p. 169.
[15] D. Linden, Handbook of Batteries, McGraw-Hill, New York, 1995, pp. 1–9.
[16] H. Kataoka, Y. Saito, T. Sakai, E. Quartarone, P. Mustarelli, J. Phys. Chem. B 104 (2000) 11460.